Monte Carlo simulation of Comptonization in inhomogeneous media

Xin-Min Hua[a)]
Laboratory for High Energy Astrophysics, NASA/GSFC Code 661, Greenbelt, Maryland 20771

(Received 2 December 1996; accepted 2 July 1997)

Comptonization is the process in which the photon spectrum changes due to multiple Compton scatterings in the electronic plasma. It plays an important role in the spectral formation of astrophysical x-ray and gamma-ray sources. There are several intrinsic limitations to the analytical method in dealing with the Comptonization problem and Monte Carlo simulation provides one of the few alternatives. We describe an efficient Monte Carlo method that can solve the Comptonization problem in a fully relativistic way. We expanded the method so that it is capable of simulating Comptonization in the media where electron density and temperature vary discontinuously from one region to the other and in the isothermal media where density varies continuously along photon paths. The algorithms are presented in detail to facilitate computer code implementation. We also present a few examples of its application to astrophysical research.
 [S0894-1866(97)02005-1]

INTRODUCTION

Comptonization—the process where the photon spectrum changes due to multiple Compton scatterings in the electronic plasma—is one of the most important processes in the spectral generation of x-ray binaries, active galactic nuclei, and other x-ray and gamma-ray sources. The analytical treatment of Comptonization is essentially based on the solution of Kompaneet's equation, which describes the interactions between the radiation field and thermal electrons.[1] Due to the mathematical complexity, however, previous analysis of Comptonization depended on simplifications such as the nonrelativistic approximation, and therefore the results were only applicable to a relatively small range of photon and electron energies.[2] In recent years, Titarchuk[3] developed a modified analytical technique that took into account the relativistic effect and Klein–Nishina corrections, thereby extending the previous work to wider ranges of temperature and optical depth of the plasma clouds from which Comptonized photons emerge.

The analytical method, however, has several intrinsic limitations. First, all analytical models are based on solving certain types of radiation transfer equations,[1] which in turn is based on the assumption that the energy and position of the photons are continuous functions of time, that is, these models assume diffusion of photons in the energy and position spaces. While the continuity of energy change is a good approximation for scatterings at low energy, it is obviously not valid for Compton scatterings at high photon energies or scattering by relativistic electrons. Similarly, the continuity of photon position change is an approximation valid only for clouds of electron plasma with dimensions that are large compared to the scattering mean free path (that is, diffusion approximation). But astronomical observations suggest that many of the sources where Comptonization is believed to take place have optical depths of the order of one Thomson scattering mean free path.

Second, solutions of the radiative transfer equations are based on the separation of photon diffusions in energy and position spaces.[2–4] The solutions can be presented in terms of simple analytical expressions only when the initial source photons have energies much lower than the electron energy and follow a particular spatial distribution, namely, the first eigenfunction of the spatial operator of the diffusion equation. It was found[4] that, for source photons at energies not far below the electron energy or for clouds with large optical depth, the emergent spectra are sensitive to both the spectral and spatial distributions of source photons, and the results of analytical method must be expanded to the higher-order terms. Consequently, the analytical models are applicable only to certain ranges of plasma temperature and optical depth where solutions are insensitive to source conditions.

Third, the analytical methods are inadequate to treat the temporal behavior of Comptonized emissions. Hua and Titarchuk[5] have shown that, for relativistic plasma, photons gain energy significantly with each scattering and consequently the scattering mean free path changes significantly with each scattering. Besides, for plasma clouds with small optical depth, the scattering mean free path is mainly determined by the boundary condition rather than by the scattering cross-sections. As a result, analytical treatment[6] is applicable only to the limited situation in which the electron plasma has nonrelativistic temperatures and optical depths much greater than the Thomson mean free path.

In addition to the above limitations, the analytical approach is totally incapable of dealing with the Comptonization problems involving complicated geometries and inhomogeneity of electronic media, where scattering mean free path depends on scattering location and direction as well as

[a)]Also with the Universities Space Research Association. E-mail: hua@milkyway.gsfc.nasa.gov

  0894-1866/97/11(6)/660/9/$10.00

on photon energy. But observations seem to indicate that investigations of Comptonization in the media with nonuniform temperature and density are necessary. As was shown by Skibo *et al.*[7] and Ling *et al.*,[8] the spectral hardening at high energies in the spectra of AGNs and black hole candidates may result from the temperature gradient in the plasmas responsible for the emissions. Kazanas *et al.*[9] and Hua *et al.*[10] showed that temporal behavior such as the hard x-ray phase lags observed from the accreting compact objects could be explained by the nonuniform electron density of the accreting gas clouds.

These situations are where the analytical method fails. As an alternative, Monte Carlo simulation can be employed to provide the solutions. Monte Carlo is flexible in simulating various initial conditions of source photons, complicated geometries, and density profiles of plasma clouds. It is capable of presenting the full spectra resulting from Comptonization rather than the asymptotic ones obtainable from analytical methods. The first attempt to use the Monte Carlo method to solve the Comptonization problem was by Pozdnyakov *et al.*[11] In recent years, Stern *et al.*[12] presented a large-particle Monte Carlo method for simulating Comptonization and other high-energy processes. Skibo *et al.*[7] used a Monte Carlo simulation in the calculation of photon spectra of mildly relativistic thermal plasmas in pair balance.

In this study, we develop an efficient Monte Carlo method that treats the Comptonization problem in a fully relativistic way and can be implemented in a desktop computer such as a Sparc workstation or Pentium PC to yield results with satisfactory statistics in CPU time of the order of minutes to hours. The algorithms are described in detail to facilitate computer code implementation. In Sec. I we introduce an improved technique of simulating Compton scattering of photons on cold electrons. In Sec. II, we describe the method for Compton scattering on hot electrons. In Sec. III, we present the method dealing with scattering in a multizone medium. In Sec. IV, we describe the simulation of Compton scatterings in media with nonuniform density profiles.

I. COMPTON SCATTERING ON COLD ELECTRONS

The Monte Carlo method described here was developed over the past several years in investigations of Compton scattering of the 2.223-MeV gamma-ray line in solar flares,[13] Compton backscattering of the 511-keV annihilation line in sources 1E1740.7–2942,[14] and in Nova Muscae.[15]

The differential cross-section of Compton scattering is given by the Klein–Nishina formula

$$\frac{d\sigma}{d\epsilon}=\frac{3\sigma_T}{4}\cdot\frac{1}{\epsilon}\left[\left(1-\frac{4}{\epsilon}-\frac{8}{\epsilon^2}\right)\ln(1+\epsilon)+\frac{1}{2}+\frac{8}{\epsilon}-\frac{1}{2(1+\epsilon)^2}\right], \tag{1}$$

where σ_T is the Thomson cross-section, $\epsilon=2E/m_ec^2$, E is the energy of incident photon, m_e is the electron rest mass, and c is the speed of light. The energy of the scattered photon, E', relative to the initial photon energy E is given by the ratio

$$r=\frac{E}{E'}=1+\frac{\epsilon}{2}(1-\cos\psi), \tag{2}$$

where ψ is the angle between incident and scattered photons. The energy distribution of the Compton-scattered photons is determined by the distribution with respect to r, which is

$$f(r)=\begin{cases}\dfrac{1}{K(\epsilon)}\left[\left(\dfrac{\epsilon+2-2r}{\epsilon r}\right)^2+\dfrac{1}{r}-\dfrac{1}{r^2}+\dfrac{1}{r^3}\right], \\ \text{for } 1\leqslant r\leqslant\epsilon+1, \\ 0 \quad \text{otherwise,}\end{cases} \tag{3}$$

where

$$K(\epsilon)=\frac{4\epsilon}{3\sigma_T}\sigma(\epsilon) \tag{4}$$

is the normalization factor.

Sampling the distribution given by Eq. (3) plays a central role in the Monte Carlo simulation of Compton scattering of photons by cold electrons. Furthermore, as will be seen below, Compton scatterings on hot electrons in our scheme will also be reduced to the simulation of Eq. (3). Therefore, the performance of the computer program for Monte Carlo simulation of Compton scatterings depends critically on the quality of the technique used for sampling this distribution because a run of the program typically involves millions of scatterings. Efforts were made to optimize the technique of sampling this distribution.[16] In our implementation, we adopted a variation of Kahn's technique first suggested by Pei.[17] The algorithm of the technique is

(1) generate three random numbers ξ_1, ξ_2, and ξ_3 uniformly distributed on (0,1);
(2) if $\xi_1\leqslant 27/(2\epsilon+29)$,
    let $r=(\epsilon+1)/(\epsilon\xi_2+1)$.
    If $\xi_3>\{[(\epsilon+2-2r)/\epsilon]^2+1\}/2$, go to 1.
    Else accept r.

  Else
    let $r=\epsilon\xi_2+1$.
    If $\xi_3>6.75(r-1)^2/r^3$, go to 1.
    Else accept r.

It is seen that this is essentially a combination of composition and rejection methods.[18] This algorithm, like Kahn's, avoids operations such as the square root, logarithm, or trigonometric functions, which involve time-consuming series expansion for computers. Its quality can also be measured to a large extent by the rejection rates, which are 0.38, 0.30, 0.23, and 0.33 for $\epsilon=0.2$, 2, 10, and 20, respectively, as compared to 0.41, 0.37, 0.41, and 0.53 for Kahn's technique. The improvement is significant, especially for higher photon energies.

II. COMPTONIZATION IN HOT ISOTHERMAL HOMOGENEOUS PLASMAS

The Monte Carlo technique for photon Comptonization in a relativistic plasma was outlined by Pozdnyakov *et al.*[11] and by Gorecki and Wilczewski.[19] Our implementation of the simulation is somewhat different from these authors. Ours was developed on the basis of the technique for Compton scattering on cold electrons described in Sec. I.

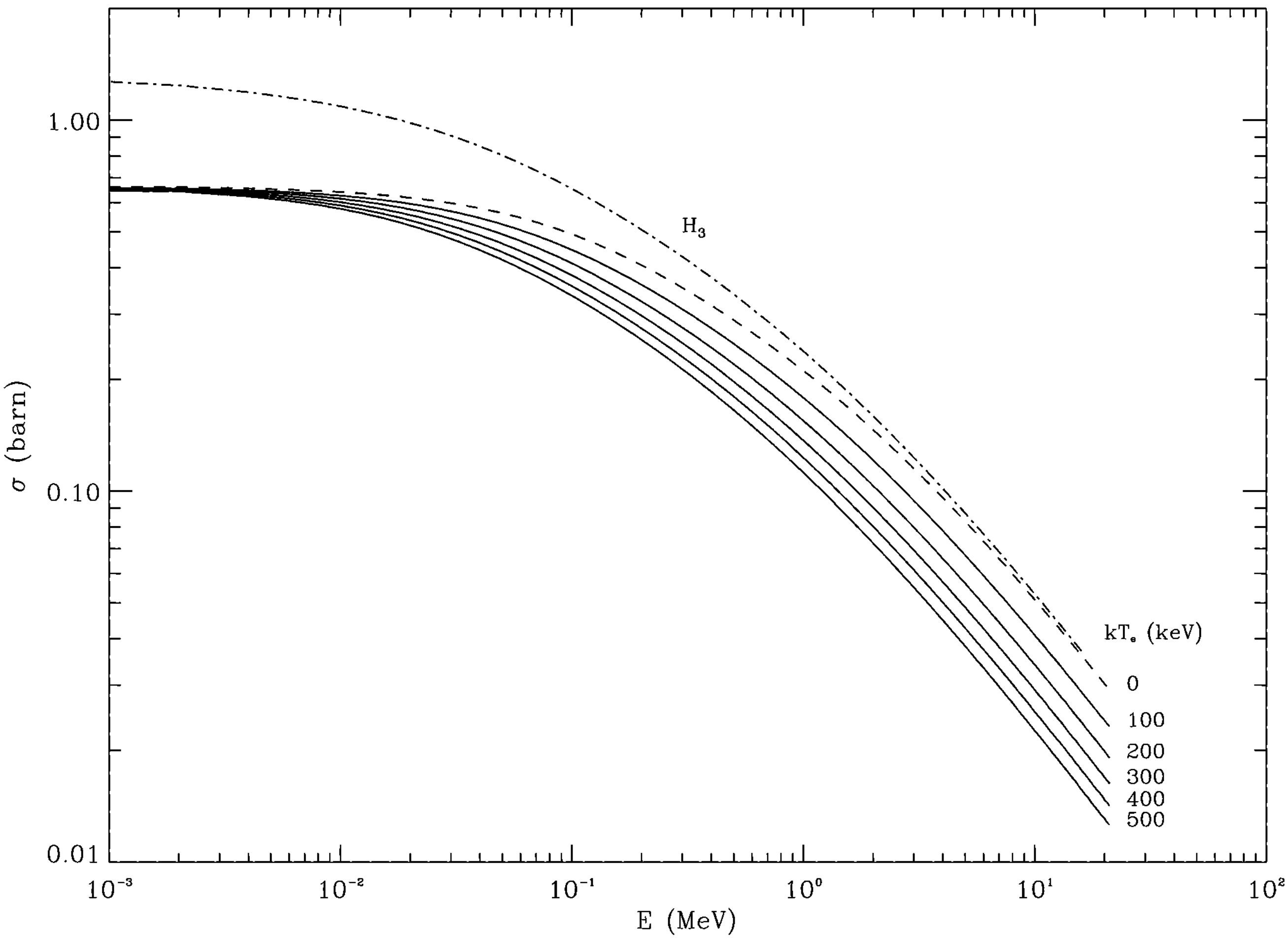

Figure 1. Maxwellian averaged Compton scattering cross-section for various plasma temperatures, obtained from numerical integration in Eq. (10). Also plotted is the maximum effective cross-section as a function of photon energy $H_3(E)$.

Let us suppose a photon is scattered off an electron that is moving in the z-axis direction with a velocity v. The energies of the incident and the scattered photon are E and E', respectively. The zenith angles of the incident and scattered photons measured from the z axis are θ and θ', respectively. ϕ and ϕ' are the azimuthal angles. The differential cross-section for Compton scattering is given by[20]

$$\frac{d\sigma}{d\mu' d\phi'} = \frac{3\sigma_T}{16\pi}\frac{1}{\gamma^2}\frac{\chi}{(1-v\mu)^2}\left(\frac{E'}{E}\right)^2, \tag{5}$$

where $\mu = \cos\theta$ and $\mu' = \cos\theta'$, v is in units of the speed of light, and $\gamma = (1-v^2)^{-1/2}$;

$$\chi = \frac{\epsilon}{\epsilon'} + \frac{\epsilon'}{\epsilon} + \frac{4}{\epsilon}\left(1-\frac{\epsilon}{\epsilon'}\right) + \frac{4}{\epsilon^2}\left(1-\frac{\epsilon}{\epsilon'}\right)^2; \tag{6}$$

$$\epsilon = \frac{2E}{m_e c^2}\,\gamma(1-v\mu), \quad \epsilon' = \frac{2E'}{m_e c^2}\,\gamma(1-v\mu'); \tag{7}$$

$$\frac{E'}{E} = \frac{1-v\mu}{1-v\mu' + (E/\gamma m_e c^2)(1-\cos\psi)}; \tag{8}$$

and ψ is the angle between incident and scattered photons $\cos\psi = \mu\mu' + \sqrt{(1-\mu^2)(1-\mu'^2)}\cos(\phi-\phi')$.

Integration over μ' and ϕ' leads to

$$\sigma(\epsilon) = \frac{3\sigma_T}{4}\cdot\frac{1}{\epsilon}\left[\left(1-\frac{4}{\epsilon}-\frac{8}{\epsilon^2}\right)\ln(1+\epsilon) + \frac{1}{2} + \frac{8}{\epsilon} - \frac{1}{2(1+\epsilon)^2}\right]. \tag{9}$$

It is seen that Eq. (9) is identical in form to Eq. (1). But the quantity ϵ here is given by the relativistic expression in Eq. (7). In other words, it is dependent on the electron's energy and direction as well as the photon's energy.

A photon with energy E traveling in a plasma with an isotropic distribution of electrons having an energy distribution $N_e(\gamma)$ will have an averaged cross-section of Compton scattering:[21]

$$\sigma_a(T_e, E) = \frac{1}{2}\int_1^\infty d\gamma \int_{-1}^{1} d\mu(1-v\mu)\sigma(\epsilon)N_e(\gamma). \tag{10}$$

For a plasma in thermal equilibrium, $N_e(\gamma)$ is the Maxwell distribution given by

$$N_e(\gamma)=\frac{1}{2\Theta K_2(1/\Theta)}\,v\gamma^2 e^{-\gamma/\Theta}, \tag{11}$$

where $\Theta=kT_e/m_e c^2$ is the dimensionless temperature of the plasma, k is the Boltzmann constant, and K_2 is the modified Bessel function of second order. The $\sigma_a(T_e,E)$ values in the form of a data matrix, obtained by the two-dimensional integration in Eq. (10) for a properly spaced array of T_e and E, can be read by or incorporated into the computer codes. Values of $\sigma_a(T_e,E)$ for several temperatures are numerically calculated and are plotted in Fig. 1. The dashed curve is the cross-section at $T_e=0$, given by the Klein–Nishina formula in Eq. (1). It can be seen that, for energetic photons scattering off the high-temperature electrons, the cross-section can be smaller by a factor of 2 or more than those scattering off the cold electrons. In other words, hot plasmas are more transparent than cold ones for photons. This has an important effect on the energy spectra emerging from such plasmas, one which Titarchuk[3] took into account in his modification of the previous analytical results. Its effect on the temporal behavior of x-ray and gamma-ray emission from these plasmas is even more significant and it was discussed by Hua and Titarchuk.[5]

With $\sigma_a(T_e,E)$ obtained by numerical integration in Eq. (10), we can use the Monte Carlo method to select the free path between two successive scatterings for a photon with energy E.

$$\int_0^{\ell} n_e\sigma_a ds=-\ln\xi, \tag{12}$$

where ℓ is the free path to be sampled, n_e is the electron density, and ξ is a uniform random number on (0,1). The integration is taken along the photon's path length s. Here we are only concerned with the isothermal plasmas at temperature T_e and with uniform density n_e and leave the discussion of inhomogeneous media to Secs. III and IV. Under this assumption, ℓ can be sampled simply by

$$\ell=-\frac{\ln\xi}{n_e\sigma_a(T_e,E)}. \tag{13}$$

At the location of scattering, an electron is selected to scatter the photon. Its energy factor γ and direction $\mu=\cos\theta$ with respect to the photon direction are selected according to the distribution

$$f_e(\gamma,\mu)\propto(1-\mu\sqrt{1-\gamma^{-2}})\sigma(\epsilon)N_e(\gamma), \tag{14}$$

while its azimuthal angle ϕ around the photon direction is selected uniformly on $(0,2\pi)$. The distribution in Eq. (14) is rather complicated because ϵ depends on γ and μ as given in Eq. (7). On the other hand, for a thermal plasma, $N_e(\gamma)$ is given by Eq. (11) and independent of μ. In our implementation of the distribution Eq. (14), we use the following algorithm:

(1) generate two random numbers ξ_1 and ξ_2 uniformly distributed on (0,1);

(2) if $\Theta\leqslant 0.01$,
  if $\xi_2^2>-e\xi_1\ln\xi_1$, go to 1.
  Else let $v=\sqrt{-3\Theta\ln\xi_1}$, $\gamma=1/\sqrt{1-v^2}$.
 Else if $\Theta\leqslant 0.25$,
  let $\gamma=1-1.5\Theta\ln\xi_1$.
  If $\xi_2 H_1>\gamma\sqrt{\xi_1(\gamma^2-1)}$, go to 1.
 Else
  let $\gamma=1-3\Theta\ln\xi_1$.
  If $\xi_2 H_2>\gamma\xi_1^2\sqrt{\gamma^2-1}$, go to 1.

(3) Generate μ uniform on $(-1,1)$ and ξ_3 uniform on (0,1).

(4) Calculate ϵ and then $\sigma(\epsilon)$ from γ and μ according to Eqs. (7) and (9).

(5) If $\xi_3 H_3>(1-\mu\sqrt{1-\gamma^{-2}})\sigma(\epsilon)$, go to 1.
 Else accept γ and μ.

Here

$$H_1=a\sqrt{a^2-1}\,\exp\left(-\frac{a-1}{3\Theta}\right), \tag{15}$$

$$a=2\Theta+2b\cos\left[\frac{1}{3}\cos^{-1}\left(\Theta\,\frac{16\Theta^2-1}{2b^3}\right)\right]$$

and

$$b=\sqrt{1/3+4\Theta^2},$$

$$H_2=a\sqrt{a^2-1}\,\exp\left(-\frac{2(a-1)}{3\Theta}\right),$$

$$A=\Theta+2b\cos\left[\frac{1}{3}\cos^{-1}\left(\Theta\,\frac{4\Theta^2-1}{4b^3}\right)\right] \tag{16}$$

and

$$b=\sqrt{1/3+\Theta^2},$$

and H_3 is the maximum of the so-called "effective cross-section" $\sigma_{\rm eff}=(1-\mu\sqrt{1-\gamma^{-2}})\sigma(\epsilon)$.

Several points should be made in the above algorithm. Steps (1) and (2) sample a candidate γ using the rejection method in terms of the Maxwellian distribution $N_e(\gamma)$, which is independent of the photon energy and direction. For low plasma temperature ($\Theta\leqslant 0.01$) electron velocity v is sampled according to the nonrelativistic Maxwellian distribution. For high temperatures, the separated sampling ($\Theta\leqslant 0.25$ and >0.25) is used in order to reduce the rejection rates. It should be emphasized that, although the expressions of H_1 and H_2 are complicated, these quantities depend on Θ alone and therefore need to be calculated once only. They can be calculated outside the scattering loop as long as the plasma temperature remains unchanged. The γ values so sampled, together with the isotropically sampled μ, represent electrons in the hot plasma at the given temperature. They are subject to another rejection test in the subsequent steps in order to yield the right joint distribution given in Eq. (14), which represents the electrons that actually scatter the photon.

The quantity H_3 is not expressible analytically. It depends on incident photon energy E only and can be determined by maximizing the effective cross-section with respect to γ and μ for any given E using numerical methods such as those given in Press *et al.*[22] In the following, we describe an alternative to the above two-dimensional maximization methods. We examine the derivative of $\sigma_{\rm eff}(\gamma,\mu)$ with respect to μ

$$\frac{\partial\sigma_{\rm eff}}{\partial\mu}=-\frac{2E}{m_e c^2}\sqrt{1-\gamma^{-2}}\,\frac{dh}{d\epsilon}, \tag{17}$$

where

$$h(\epsilon)=\left(1-\frac{4}{\epsilon}-\frac{8}{\epsilon^2}\right)\ln(1+\epsilon)+\frac{1}{2}+\frac{8}{\epsilon}-\frac{1}{2(1+\epsilon)^2} \tag{18}$$

is the expression in the square brackets in Eq. (9). It can be easily verified that

$$\frac{\partial\sigma_{\rm eff}}{\partial\mu}\leqslant 0,\quad \text{for } E>0 \quad \text{and} \quad \gamma\geqslant 1. \tag{19}$$

Therefore, $\sigma_{\rm eff}(\gamma,\mu)$ is a monotonously decreasing function of μ, that is, for given γ, $\sigma_{\rm eff}(\gamma,\mu)$ reaches its maximum at $\mu=-1$. Physically, this means that a head-on collision between the photon and electron always has a maximum probability. Thus, in order to determine the maximum of $\sigma_{\rm eff}$ as a function of γ and μ, one only needs to maximize the one-dimensional function $\sigma_{\rm eff}(\gamma,-1)$. The maximum of $\sigma_{\rm eff}$, or H_3, as a function of E determined in this way is plotted in Fig. 1 as the dash-dotted curve. It is seen that, for high photon energies, the maximum effective cross-section approaches the Klein–Nishina cross-section while at low energies it approaches twice the Thomson cross-section. The H_3 values for an array of properly spaced E values can be tabulated and incorporated into the computer codes.

With the selected electron energy and direction represented by γ, μ, and ϕ uniform on $(0,2\pi)$, we proceed to determine the energy and direction of the scattered photon. In order to do so, we simulate Compton scattering in the frame where the electron before scattering is at rest rather than sampling the multivariate distribution of E', μ', and ϕ' from Eq. (5). The Lorentz transformation of the photon momentum between this reference frame and the lab frame is given by

$$\mathbf{p}'=\mathbf{p}-p[\gamma v-(\gamma-1)\hat{\mathbf{p}}\cdot\hat{\mathbf{v}}]\hat{\mathbf{v}}, \tag{20}$$

where $\mathbf{p}$ and $\mathbf{p}'$ are photon momentum vectors before and after the transformation, and $\hat{\mathbf{p}}$ and $\hat{\mathbf{v}}$ are unit vectors of the photon momentum and electron velocity, respectively.

In the electron rest frame, we utilize the Monte Carlo method described in Sec. I. The resulting momentum of the scattered photon is then transformed back to the lab frame using the same Eq. (20) with a reversed $\hat{\mathbf{v}}$. The energy and direction of the scattered photon obtained in this way automatically satisfy the energy conservation relationship given in Eq. (8).

As a crucial test we ran the program in which low-frequency photons were allowed to scatter in an infinite plasma at a given temperature for a sufficiently long time. It was expected that the photon energy should approach the Wien distribution at the given plasma temperatures. One example of such evolution, the photon energy distribution recorded at varies times in a plasma of $kT_e=200$ keV, is shown in Fig. 2. It does approach the Wien form.

III. COMPTONIZATION IN MULTIZONE MEDIA

If Comptonization takes place in a medium that is divided into several zones each with different electron temperatures and density distributions, one has to take into consideration the boundaries between these zones in addition to the scattering free paths and the boundary of the entire medium.

In general, suppose a photon, after initiation or scatterings, is located in the medium at (x_0,y_0,z_0) with a direction $(\omega_1,\omega_2,\omega_3)$. The next position where the photon will scatter, if there were no boundaries, is given by

$$\begin{cases} x_1=x_0+\ell\omega_1\\ y_1=y_0+\ell\omega_2\\ z_1=z_0+\ell\omega_3, \end{cases} \tag{21}$$

where ℓ is sampled according to Eq. (13), in which n_e and T_e should be understood as the electron density and temperature in the present zone. With the existence of boundaries, (x_1,y_1,z_1) could be in the neighboring zone or outside of the medium. In this case, one has to calculate the distances s_i from (x_0,y_0,z_0) to various boundaries B_i $(i=1,\dots,N)$, where N is the number of boundaries surrounding the zone under consideration. s_i can be obtained by solving the equations describing the ith boundary

$$B_i(x,y,z)=0,\quad i=1,\dots,N, \tag{22}$$

where

$$\begin{cases} x=x_0+s_i\omega_1\\ y=y_0+s_i\omega_2\\ z=z_0+s_i\omega_3. \end{cases} \tag{23}$$

If ℓ is smaller than any of $s_1,\dots s_N$ obtained, the photon will remain in the same zone and scatter at the location (x_1,y_1,z_1) on electrons at local temperature T_e. But if s_j is the minimum among ℓ and $s_1,\dots s_N$, the photon will hit the boundary B_j. In this case one has to replace the photon on the boundary at (x,y,z) determined by Eq. (23) with $i=j$. With the new position on the boundary as (x_0,y_0,z_0), one can begin another round of free path sampling with n_e and T_e of the zone the photon is entering while keeping the photon energy and direction unchanged.

In the study of gamma-ray spectra of Cygnus X-1,[8] we developed a model where photons scatter in a two-layered spherical plasma consisting of a high-temperature core and a cooler corona. The model was first proposed by Skibo and Dermer[23] to interpret the x-ray spectral hardening at high energies observed in active galactic nuclei (AGNs). The boundary of the inner core is a sphere of radius R_i while the boundaries of the outer shell are two spheres with radii R_i and R_o, respectively. For a photon in the core, the equation for the distance s_1 to its boundary is

$$s_1^2+2(\mathbf{r}_0\cdot\hat{\omega})s_1-(R_i^2-r_0^2)=0, \tag{24}$$

where $\mathbf{r}_0=(x_0,y_0,z_0)$ is the position vector of the photon and $\hat{\omega}=(\omega_1,\omega_2,\omega_3)$. Similarly, the equations for a photon in the outer shell are

$$\begin{cases} s_1^2+2(\mathbf{r}_0\cdot\hat{\omega})s_1-(R_i^2-r_0^2)=0\\ s_2^2+2(\mathbf{r}_0\cdot\hat{\omega})s_2-(R_o^2-r_0^2)=0. \end{cases} \tag{25}$$

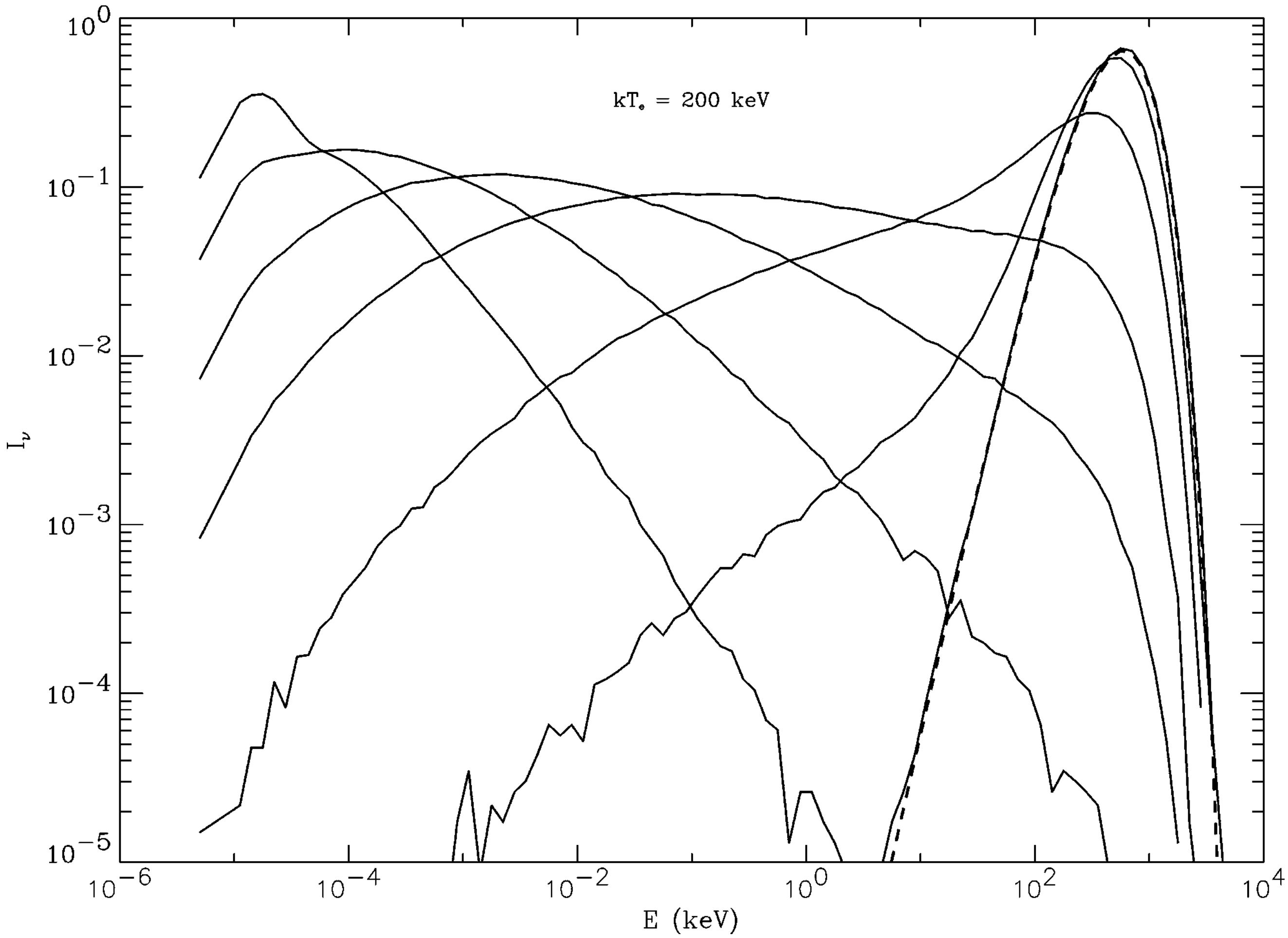

Figure 2. The evolution of photon energy distribution from a blackbody at 0.511×10^{-2} eV towards equilibrium with a plasma at kT_e=200 keV. The seven spectra (solid curves) are ''snapshots'' at times $t=1$, 3, 6, 10, 18, 30, and 70 Thomson mean free time. Also plotted (dashed curve) are the Wien spectra at a temperature of 200 keV.

Thus we have the following algorithm:

if $r_0<R_i$,
  let $\delta=(\mathbf{r}_0\cdot\hat{\omega})^2+(R_i^2-r_0^2)$ and $s_1=\sqrt{\delta}-(\mathbf{r}_0\cdot\hat{\omega})$.
  If $\ell<s_1$, scatter at $\mathbf{r}_1=\mathbf{r}_0+\ell\hat{\omega}$.
  Else reach boundary at $\mathbf{r}_1=\mathbf{r}_0+s_1\hat{\omega}$.
Else if $r_0<R_o$,
  let $\delta=(\mathbf{r}_0\cdot\hat{\omega})^2+(R_i^2-r_0^2)$.
  If $\delta\geqslant0$ and $(\mathbf{r}_0\cdot\hat{\omega})<0$,
    let $s_1=-\sqrt{\delta}-(\mathbf{r}_0\cdot\hat{\omega})$.
    If $\ell<s_1$, scatter at $\mathbf{r}_1=\mathbf{r}_0+\ell\hat{\omega}$.
    Else reach boundary at $\mathbf{r}_1=\mathbf{r}_0+s_1\hat{\omega}$.
  Else
    Let $\delta=(\mathbf{r}_0\cdot\hat{\omega})^2+(R_o^2-r_0^2)$ and $s_2=\sqrt{\delta}-(\mathbf{r}_0\cdot\hat{\omega})$.
    If $\ell<s_2$, scatter at $\mathbf{r}_1=\mathbf{r}_0+\ell\hat{\omega}$.
    Else escape.

Whenever the photon crosses the inner boundary, the plasma density and temperature should be switched and the photon energy and direction should be the same.

In Fig. 3, we present the result of such a calculation (solid curve) together with the observational data[8] it was intended to fit. The data were from the black hole candidate Cygnus X-1 observed by the detector BATSE on board the satellite known as the Compton Gamma-Ray Observatory. The fitting spectrum was obtained from a calculation with the two-layer model described above, where the temperature is $kT_e=230$ keV for the inner core and 50 keV for the outer shell. The two zones are assumed to have the same electron density and the inner core has a radius 0.36 in units of Thomson mean free path, while the outer shell radius is 1.3. The initial photons have a blackbody temperature of 0.5 keV and are injected into the medium from outside. For comparison the best fit one can achieve by a single-zone plasma model is also presented (dashed curve). The model consists of a plasma sphere of radius 1.35 at $kT_e=85$ keV. The reduced χ^2 value is 2.6 for the single-temperature model as compared to 1.0 for the double-layer model. It is seen that, by adding a hot central core to the Comptonization medium, the fit to the high-energy part of the observed spectrum is significantly improved.

IV. COMPTONIZATION IN ISOTHERMAL MEDIA WITH NONUNIFORM DENSITY

The media we considered so far are uniform, at least regionally, in density. It was found to be necessary to inves-

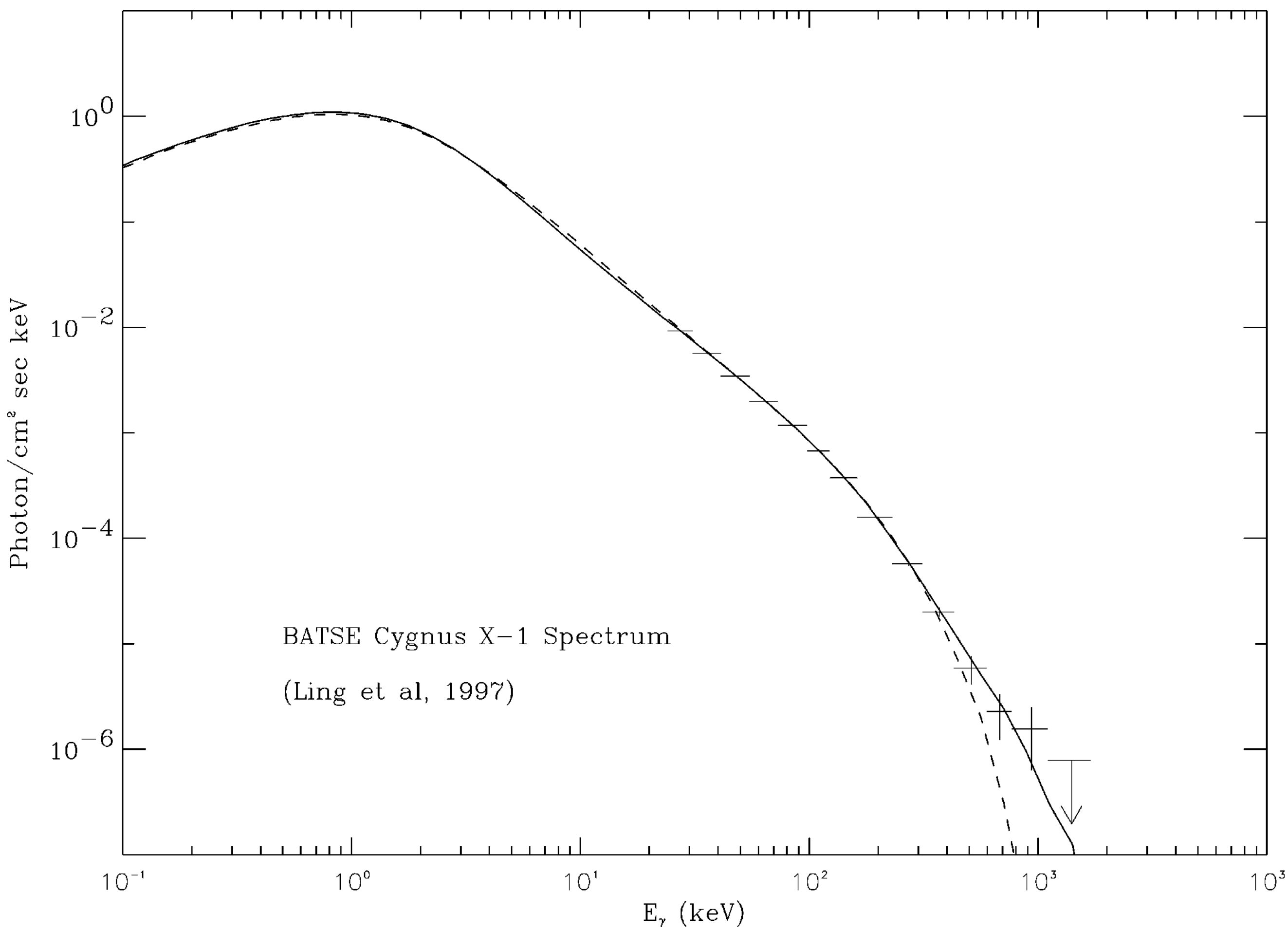

Figure 3. The energy spectra resulting from the double-layer Comptonization media (solid curve) and single-temperature sphere (dashed curve). Both spectra are intended to fit the observational data from the black hole candidate Cygnus X-1 (Ref. 8).

tigate the Comptonization in media with nonuniform density profiles.[9] We now present the treatment of two spherically symmetrical configurations commonly found in the astrophysical environment, one with electron density varying as ρ^{-1} and the other as $\rho^{-3/2}$, where ρ is the distance from the sphere center. The latter case represents the density profile of a gas free-falling onto a central accreting object under gravitational force,[24] while the former represents that of an accreting gas with viscosity due to the interaction between the gas and the outgoing photons.[9]

With density n_e varying along the photon's path length s, the integration in Eq. (12) should be written as

$$I=\int_0^{\ell} n_e(s)\sigma_a ds, \tag{26}$$

where the dependence of n_e on s is given by

$$n_e(s)=\begin{cases} \dfrac{n_0\rho_0}{\sqrt{r_0^2+s^2+2sr_0\nu}} & \text{for } \rho^{-1} \text{ profile,} \\ \dfrac{n_0\rho_0^{3/2}}{(r_0^2+s^2+2sr_0\nu)^{3/4}} & \text{for } \rho^{-3/2} \text{ profile,} \end{cases} \tag{27}$$

where ρ_0 is the radius of the sphere within which the density profiles break down, n_0 is the electron density at this radius, $\nu=(\mathbf{r}_0\cdot\hat{\omega})/r_0$, $\mathbf{r}_0$ is the photon's position vector originating from the sphere center, and $\hat{\omega}$ is its travel direction.

By substituting $n_e(s)$ in Eq. (27) into Eq. (26) we obtain the integration for ρ^{-1} profile

$$I=n_0\rho_0\sigma_a \ln\left(\frac{\ell-r_0\nu+\sqrt{\ell^2+r_0^2+2\ell r_0\nu}}{r_0(1-\nu)}\right). \tag{28}$$

Equation (12) then becomes $I=-\ln\xi$. Solving this equation for ℓ, we obtain

$$\ell=r_0\,\frac{(1+\nu)\eta^2+2\nu\eta-(1-\nu)}{2\eta}, \tag{29}$$

where $\eta=\exp(-\ln\xi/n_0\rho_0\sigma_a)$. Once a uniform random ξ is selected on (0,1), ℓ is determined by Eq. (29).

For the $\rho^{-3/2}$ density profile, the counterpart of Eq. (28) is

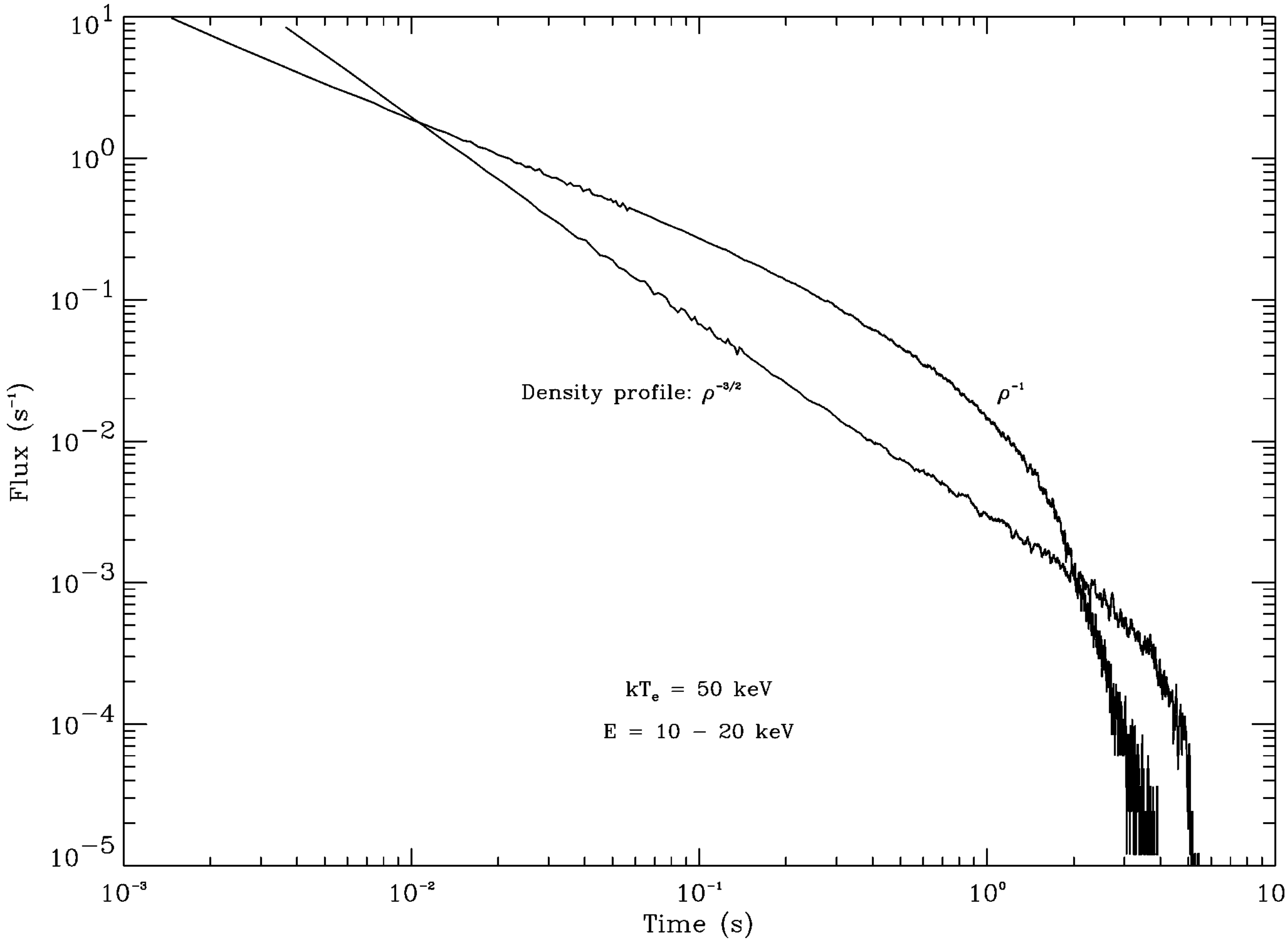

Figure 4. The light curves resulting from the core-atmosphere models. The atmospheres have ρ^{-1} and $\rho^{-3/2}$ density profiles, respectively.

$$I=n_0\rho_0\sigma_a\sqrt{\frac{2\rho_0}{r_0 \sin \vartheta}}\left[F\left(\varphi_\ell,\frac{1}{\sqrt{2}}\right)-F\left(\varphi_0,\frac{1}{\sqrt{2}}\right)\right], \tag{30}$$

where $F(\varphi,k)$ is the Legendre elliptic integral of the first kind, $\sin \vartheta=\sqrt{1-\nu^2}$, φ_0 and φ_ℓ are given by

$$\begin{cases}\cos \varphi_0=(1+u_0^2)^{-1/4}\\ \cos \varphi_\ell=(1+u_\ell^2)^{-1/4},\end{cases} \tag{31}$$

and

$$\begin{cases}u_0=\dfrac{\cos \vartheta}{\sin \vartheta}\\ u_\ell=\dfrac{\ell+r_0 \cos \vartheta}{r_0 \sin \vartheta}.\end{cases} \tag{32}$$

Substituting the integration into Eq. (12), we obtain

$$F\left(\varphi_\ell,\frac{1}{\sqrt{2}}\right)=F\left(\varphi_0,\frac{1}{\sqrt{2}}\right)-\frac{\ln \xi}{n_0\rho_0\sigma_a}\sqrt{\frac{r_0 \sin \vartheta}{2\rho_0}}, \tag{33}$$

where the right-hand side is a function of known variables. Let us call it $f(\xi,r_0\vartheta)$. We solve Eq. (33) and obtain

$$\cos \varphi_\ell=\mathrm{cn}\left(f,\frac{1}{\sqrt{2}}\right), \tag{34}$$

where $\mathrm{cn}(f,k)$ is the Jacobian elliptic function, which is the inverse of the elliptic integral $F(\varphi_\ell,k)$. Computer routines for both elliptic integral and Jacobian elliptic functions are available in many mathematical libraries.[22] Finally, ℓ can be obtained from Eqs. (31) and (32)

$$\ell=r_0 \sin \vartheta\sqrt{\mathrm{cn}^{-4}\left(f,\frac{1}{\sqrt{2}}\right)-1}-r_0 \cos \vartheta. \tag{35}$$

Once ℓ is available, one can use the algorithms described in Sec. III to determine if the photon scatters, escapes, or hits the boundary.

We used ℓ given in Eqs. (29) and (35) to study the Comptonization in a two-layer spherical model similar to that in Sec. III but with the outer layer having a ρ^{-1} or $\rho^{-3/2}$ density profile. Specifically, we assume the density in the outer shell is given by Eq. (27) with $\rho_0=R_i$ and the density of the inner core is constant n_+. It is found that the energy spectrum of the x rays emerging from such a system is different from a uniform sphere with the same optical depth.[9] More important, with the decreasing density profiles, the outer layer, or the ''atmosphere,'' can extend to a distance much greater than the size a uniform system with the same optical depth can, giving rise to the time variability on a much greater time scale.

As an example, we show in Fig. 4 two light curves, or the time-dependent fluxes, for x-ray photons escaping from two such core-atmosphere systems, one with a ρ^{-1} and the other with a $\rho^{-3/2}$ density profile for the atmospheres. For both density profiles, the temperature is 50 keV in the atmosphere as well as in the core; the total optical depth is 2 in terms of Thomson scattering and the radius of the inner cores is assumed to be 2×10^{-4} light seconds. The core density n_+ is slightly different in each, 1.6×10^{17} and $1.68\times10^{17}\ \mathrm{cm}^{-3}$ for the ρ^{-1} and $\rho^{-3/2}$ profiles, respectively. For the outer atmospheres, n_0 in Eq. (27) are 0.4×10^{17} and $1.68\times10^{17}\ \mathrm{cm}^{-3}$ for the systems, respectively. As a result the radii of the systems are 1.01 and 2.63 light seconds, respectively.

Photons of a blackbody spectrum at a temperature of 2 keV are injected into the system at the center. The Comptonized photons in the energy range 10–20 keV are collected according to their escape time, and the light curves produced are displayed in Fig. 4. It is seen that these light curves are power laws extending to the order of seconds followed by exponential cutoffs. The indices of the power law are roughly 1 and 3/2, respectively, which was explained in Kazanas *et al.*[9] This temporal behavior differs greatly from the light curves from a uniform system, which decay exponentially from the very beginning of the emissions.[5] In addition, for a uniform system of similar optical depth and an electron density of the order of 10^{16} or $10^{17}\ \mathrm{cm}^{-3}$, the characteristic decay time of the light curves will be ~1 ms. The implication of the prolonged power-law light curves resulting from the extended atmosphere models for the interpretation of the recent x-ray observational data is discussed elsewhere.[9,10]

V. SUMMARY

We have shown that the analytical method has intrinsic limitations in dealing with the Comptonization problem and Monte Carlo simulation provides a useful alternative. We have introduced an efficient Monte Carlo method that can solve the Comptonization problem in a truly relativistic way. The method was further expanded to include the capabilities of dealing with Comptonization in media where electron density and temperature vary discontinuously from one region to the other and in isothermal media where density varies continuously along the photon paths. In addition to the examples given above for its application, the method was also used in the investigation of Compton scattering of gamma-ray photons in accretion disks near black hole candidates[14] and in the Earth's atmosphere and the spacecraft material.[25]

ACKNOWLEDGMENTS

The author would like to thank R. E. Lingenfelter and R. Ramaty for their long-term support and encouragement in the past decade during which the technique described here was developed. The author would also like to thank J. C. Ling, L. Titarchuk, and D. Kazanas for valuable discussions and NAS/NRC for support during the period of this study.

REFERENCES

1. A. S. Kompaneets and Zh. Eksper, Teoret. Fiz. **31**, 876 (1956) [Sov. Phys. JETP **4**, 730 (1957)].
2. R. A. Sunyaev and L. G. Titarchuk, Astron. Astrophys. **86**, 121 (1980).
3. L. Titarchuk, Astrophys. J. **434**, 570 (1994).
4. X.-M. Hua and L. Titarchuk, Astrophys. J. **449**, 188 (1995).
5. X.-M. Hua and L. Titarchuk, Astrophys. J. **469**, 280 (1996).
6. D. G. Payne, Astrophys. J. **237**, 951 (1980).
7. J. G. Skibo, C. D. Dermer, R. Ramaty, and J. M. Mc Kinley, Astrophys. J. **446**, 86 (1995).
8. J. C. Ling, W. A. Wheaton, P. Wallyn, W. A. Mahoney, W. S. Paciesas, B. A. Harmon, G. J. Fishman, S. N. Zhang, and X.-M. Hua, Astrophys. J. **484**, 375 (1997).
9. D. Kazanas, X.-M. Hua, and L. Titarchuk, Astrophys. J. **480**, 735 (1997).
10. X.-M. Hua, D. Kazanas, and L. Titarchuk, Astrophys. J. **482**, L57 (1997).
11. L. A. Pozdnyakov, I. M. Sobol, and R. A. Sunyaev, in *Astrophysics and Space Physics Reviews*, Soviet Scientific Reviews Vol. 2, edited by R. A. Sunyaev (1983), p. 189.
12. B. E. Stern, M. C. Begelman, M. Sikora, and R. Svensson, Mon. Not. R. Astron. Soc. **272**, 291 (1995).
13. X.-M. Hua, Ph.D. thesis, University of California, San Diego, 1986.
14. R. E. Lingenfelter and X.-M. Hua, Astrophys. J. **381**, 426 (1991).
15. X.-M. Hua and R. E. Lingenfelter, Astrophys. J. **416**, L17 (1993).
16. H. Kahn, Application of Monte Carlo (AECU-3259) (1954).
17. L.-C. Pei, KEJI **4**, 374 (1979) (in Chinese).
18. B. D. Ripley, *Stochastic Simulation* (Wiley, New York, 1987).
19. A. Gorecki and W. Wilczewski, Acta Astron. **34**, 141 (1984).
20. A. I. Akhiezer and V. B. Berestetskii, *Quantum Electrodynamics* (Nauka, Moscow, 1969).
21. L. D. Landau and E. M. Lifshits, *The Classical Theory of Fields*, 4th ed. (Pergamon, New York, 1976).
22. W. H. Press, S. A. Teukolsky, W. T. Vetterling, and B. P. Flannery, *Numerical Recipes* (Cambridge University Press, Cambridge, 1992).
23. J. G. Skibo and C. D. Dermer, Astrophys. J. **455**, L25 (1995).
24. R. Narayan and I. Yi, Astrophys. J. **428**, L13 (1994).
25. X.-M. Hua and R. E. Lingenfelter, Proceedings of Compton Observatory Symposium, 1993, p. 927.